High-Speed All-Silicon Double Microring Avalanche Photodetectors

Yiwei Peng
Hewlett Packard Labs
Hewlett Packard Enterprise
Milpitas, CA
yiwei.peng@hpe.com

Yuan Yuan
Hewlett Packard Labs
Hewlett Packard Enterprise
Milpitas, CA
yuan.yuan@hpe.com

Wayne V. Sorin
Hewlett Packard Labs
Hewlett Packard Enterprise
Milpitas, CA
wayne.sorin@hpe.com

Stanley Cheung
Hewlett Packard Labs
Hewlett Packard Enterprise
Milpitas, CA
stanley.cheung@hpe.com

Zhihong Huang
Hewlett Packard Labs
Hewlett Packard Enterprise
Milpitas, CA
zhihong.huang@hpe.com

Marco Fiorentino
Hewlett Packard Labs
Hewlett Packard Enterprise
Milpitas, CA
marco.fiorentino@hpe.com

Raymond G. Beausoleil
Hewlett Packard Labs
Hewlett Packard Enterprise
Milpitas, CA
ray.beausoleil@hpe.com

***Abstract*—We demonstrate a novel all-Si double microring avalanche photodiode with peak responsivity of 1.65 A/W, low dark current of 3 nA before breakdown, ultra-high bandwidth of 55 GHz and data rate of 128 Gb/s.**

Keywords—microwave photonics, silicon photonics, avalanche photodiode, coupled microring resonator

I. Introduction

The explosive growth of transmission capacity in optical-fiber communication systems requires transceivers supporting baud rate over 100 Gb/s, which has led to the development of the high-speed photonic interconnects to keep the bandwidth scalable [1]. Due to the mature CMOS manufacturing techniques, the cost-effective and large-scale silicon (Si) photonics is considered as the most attractive solution for photonic interconnect and the future generation of data processors [2]. Numerous works have been done in high speed photodetection on silicon photonics platform using heteroepitaxial growth of germanium (Ge) or heterogeneous integration of III-V materials [3,4]. However, these methods need added material costs and extra process steps. Recently, all-Si avalanche photodiodes (APDs) have attracted a lot of interests for datacom applications due to its simple material system. Microring resonator (MRR) APD, benefits from optical resonant enhancement (RE) of two-photon absorption (TPA) and photon-assisted tunnelling (PAT), makes it possible to improve sub-bandgap wavelengths absorption [5, 6]. Additionally, MRR APDs have the inherent advantages of low dark current, compact size, and no need for process modifications. However, the MRR APD have inherently limited bandwidth which is determined by the cavity photon lifetime.

In here, we propose a novel double MRR APD structure offering wide passband and large bandwidth, which can break the limitation of the single MRR APD. In addition, the coupled MRR structure has a high stopband rejection and low channel crosstalk, which is suitable as a demultiplexer (DEMUX) in a wavelength division multiplexing (WDM) system. We simulate and experimentally demonstrate a 128 Gb/s all-Si MRR APD with a total responsivity of up to 1.65 A/W, a low dark current of 3 nA just before the breakdown and an ultra-high bandwidth of 55 GHz. This work proves the feasibility of new receiver (Rx) solution and can be included into silicon photonics process design kit (PDK).

II. Analytic Model

The schematic of the all-Si double MRR APD is shown in Fig. 1(a). For this structure, the first MRR is designed with a high quality factor (Q) for low loss and the second MRR is doped for photodetection. The dimension of two MRRs are the same and the racetrack structure is adopted for high coupling coefficient.

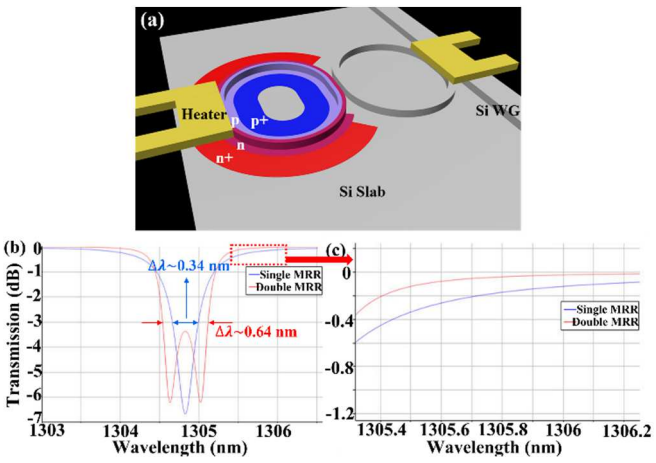

Fig.1. (a) Schematic of the double MRR APD. (b) Spectrum and (c) enlarged spectrum of a MRR APD and double MRR APD.

In Lumerical Interconnect, the power spectrums in the resonator for single and double MRR structures are simulated and shown in Fig. 1 (b) and (c). For MRR structure, electrical bandwidth is closely related to the photon lifetime and the full width at half-maximum (FWHM), Δλ of the cavity. When the similar coupling coefficient are used, the double MRR structure demonstrates around twice wider spectrum compared to the single MRR structure, which indicates that it has broader cavity enhancement region and can be adopted as an APD for a higher bandwidth. The enlarged transmission

spectrum at the through port shows that the double MRR structure benefits in terms of band sharpness and neighbor channel rejection. Compared to conventional single MRR, the double MRR APD have ~ 50% improvement on the channel crosstalk for channel spacing from 100 GHz to 200 GHz. Broadband spectrum and low channel distortion make double MRR structure suitable for WDM Rx application.

To completely understand the performance, we derive the small-signal response of the double MRR PD from the rate equation [7] as:

$$H_{AC}(\omega_m) = \frac{R}{T_{rt}E_0}\frac{2\mu_0^2\mu_1^2\delta E_0}{\mu_1^2+\gamma_r\gamma_{e2}}\left[\frac{1}{\mu_1^2+(j\omega_m+\gamma_r)(j\omega_m+\gamma_{e2})}\right] \quad (1)$$

where $R, E_0, \delta E$ and T_{rt} are the PAT coefficient, input amplitude in waveguide, modulated amplitude and round-trip transit time; μ_0 and μ_1 are the energy coupling coefficient from bus waveguide to the first MRR and from the first MRR to the second MRR; γ_r and γ_{e2} is the total amplitude decay rate in the first MRR and the amplitude decay rate due to the intrinsic loss in the second MRR.

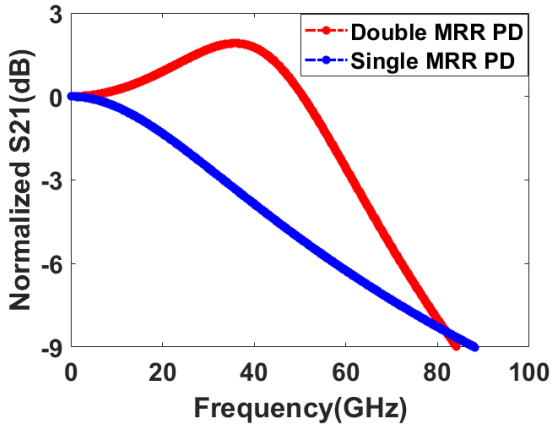

Fig.2. Simulated frequency response of double and single MRR APD

Based on the equation, the frequency responses of the MRR APD with 7.5 μm radius is calculated and shown in Fig. 2. Both double MRR and single MRR PD are biased at center wavelength and simulated with the same MRR cavity loss. Compared to single MRR PD shown as the blue lines with ~35 GHz bandwidth, double MRR PD can achieve higher bandwidth to ~60 GHz. The peaking effect on S21 can be observed due to the higher optical cavity enhancement at ~40 GHz, which corresponds to the simulated spectrums dips in the Fig. 1(b).

III. Device Design and Measured Results

A. Device Design

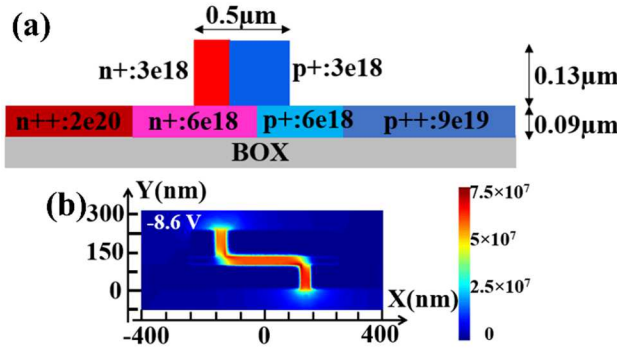

Fig. 3. (a) Schematic cross section of all-Si MRR APD. (b) Simulated electric field of the PN junction at -8.6 V.

The MRR APD consists of two 7.5 μm radius ring resonator. The ridge waveguide is formed with 220-nm height and 500-nm width. A racetrack configuration was adopted to realize ~26 % power coupling between the first MRR and bus WG. As the junction cross section shows in Fig. 3(a), the "Z" shape PN junction is created with two heavy P and N doping concentration of 6×10^{18} cm^{-3} and two light P and N doping concentration of 3×10^{18} cm^{-3}. With the presence of the new doping concentration, the junction interface enables a better overlap by ~40% between the high electric field and the optical mode and improve the absorption probability. Figure 3(b) shows the simulated electric field distribution at -8.6 V in the MRR, where the PAT effect can induce non-negligible photocurrent with the narrower junction barrier [8]. In addition, the highest electric field is 7.5×10^7 V/m, which is sufficient for impact ionization to boost the photocurrent.

B. Measured Results

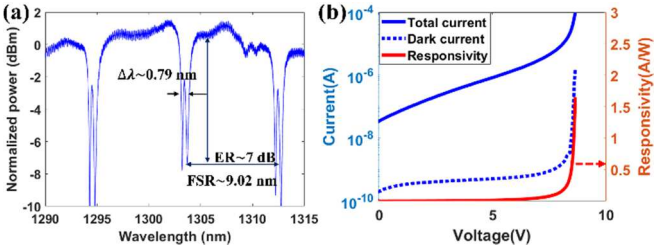

Fig. 4. (a) Normalized transmission spectrum at zero bias voltage. (b) Measured total and dark current.

We prove the feasibility of the all-Si double MRR APD in a standard Si photonics process at the Advanced Micro Foundry (AMF). A TiN pad is used as a heater to match the resonance of the two MRRs and compensate the fabrication error. From the spectrum, the MRR APD exhibits a free spectral range (FSR) of ~ 9.02 nm, a DC extinction ratio (ER) of ~ 7 dB, and a Δλ of ~ 0.79 nm. As shown in the spectrum, double MRR APD demonstrates sharper roll-off characteristic and the channel crosstalk is 50 % less than single MRR APD [9]. The suppressed crosstalk can enable 8 channels operation as a DWDM link while single MRR APD based Rx can only support 5 channels operation.

The I-V characteristics are measured at the center resonance wavelength as illustrated in Fig. 4(b), where the solid blue line is the total current, the dash blue line is the dark current, and the solid red line is responsivity. Thanks to the mature Si process, the all-Si APD demonstrates a very low dark current of only ~ 3 nA when responsivity is 0.7 A/W at -8.5 V. The highest responsivity is ~ 1.65 A/W at -8.68 V, where the dark current is 1 μA and input optical power is -12.4 dBm. It should be mentioned the responsivity can be higher under the lower optical power. As a comparison, the double MRR APD with conventional PN junction shows the peak responsivity of ~1.1 A/W. The "Z" shape implantation is verified to improve 40 % photon absorption. The PAT, cavity enhancement and avalanche gain contribute the overall sub-wavelength total responsivity.

To better understand the MRR device, the avalanche gain value is extracted according to a model that consists of three main mechanisms in [8, 10]. Based on the model, the photocurrent can be fitted when the bias voltage is selected between -2.8 V and -5.2 V, where the electric field is not high enough to trigger avalanche. As shown in Fig. 5(a), the PAT

coefficient defined in [8] is fitted to be 2.7 nm^{-1}, which is very close to the calculated value of 2.9 nm^{-1}. Dividing the fitted PAT-induced photocurrent and simulated RE from the whole photocurrent, the avalanche gain can be extracted. The gain can reach up to 9.5 at -8.4 V, 16 at -8.5 V and 46 at -8.68 V. Overall, the PAT converts ~0.4 % light to photocurrent per round-trip inside the cavity, and the MRR enhancement effect (~9×) and the avalanche gain (~46×) boost the maximum responsivity.

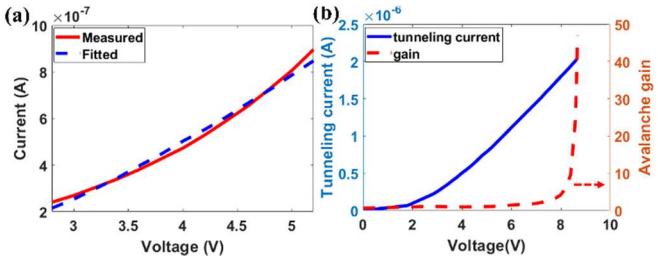

Fig. 5. (a) Measured and fitted photocurrent. (b) Extracted MRR enhanced PAT current and avalanche gain.

The frequency response of the MRR APD at different bias voltage are shown in Fig. 6(a). At each bias voltage, the S21 response was measured at the center resonance wavelength. At -7.5 V, the APD shows 3 dB bandwidth of ~ 55 GHz, which is close to the calculated photon lifetime limited bandwidth. The bandwidth is record high for all-Si MRR APD and it verifies the frequency response enhancement of double MRR structure. The bandwidth decreases to 47 GHz at -8.4 V and 25 GHz at -8.5 V, where the avalanche built-up time starts to dominate the bandwidth limitation. The GBP is 448 GHz at -8.4 V and 390 GHz at -8.5 V, which is comparable to the conventional Si-Ge APDs.

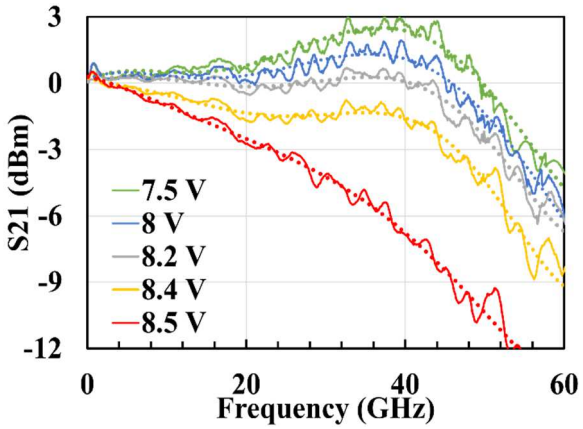

Fig. 6. Normalized frequency response of the all-Si double MRR APD.

High-speed non-return-to-zero eye diagrams were measured with pseudo random bit sequence 9 (PRBS9) signals at -8.4 V and -8.5 V. The modulated signal was applied by an arbitrary waveform generator (AWG), amplified by a praseodymium-doped fiber amplifier (PDFA) to compensate for the system losses, and detected by a MRR APD without an external transimpedance amplifier (TIA). The produced eye diagrams were recorded using a digital sampling oscilloscope (DCA) as shown in Fig. 7. Because there is no optical filter after the PDFA, the amplified spontaneous emission (ASE) noise leads to relatively high noise at both "0" and "1" levels. All eye diagrams shown here are averaged by 64 times to reduce the ASE noise. Due to the high bandwidth, the MRR APD thus can support open eye diagrams of 80 Gb/s NRZ with a signal-to-noise ratio of 5 at -8.4 V and 3.5 at -8.5 V without equalization. With a linear 8-tap feed forward equalizer (FFE), the measured SNR at -8.5 V was improved to 4.5 as shown in the bottom row. The all-Si MRR APD also has sufficient bandwidth and amplitude to support 128 Gb/s PAM4 eye diagrams without equalization. Moreover, the high-speed eye diagrams can be improved by adding a tunable optical filter to suppress the noise or integrating a TIA to enhance optical modulation amplitude.

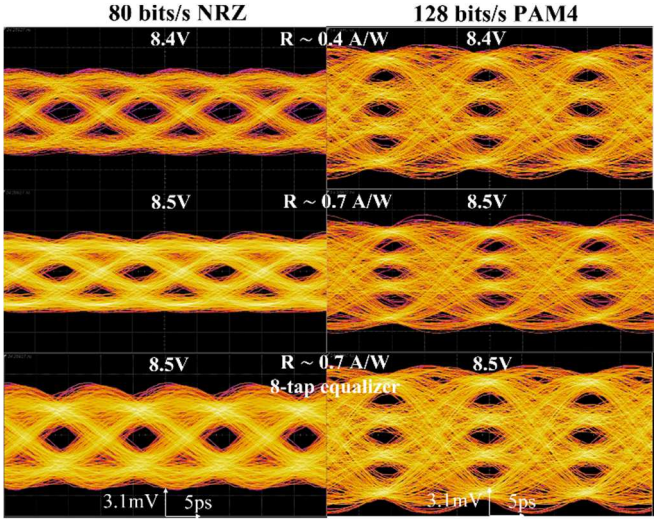

Fig. 7. The 80 Gb/s NRZ and 128 Gb/s PAM4 eye diagrams of all-Si double APDs. From top to bottom: measured at 8.4 V, 8.5 V without equalizer, and at 8.5 V with 8-tap equalizer.

The comparison of different PDs/APDs is demonstrated in Table 1. Compared to other all-Si APD, the novel double MRR structure demonstrates advantages in terms of the bandwidth. It should be noted that the implantation is designed for modulators. For the next tapeout with dedicated implantation condition, the responsivity is estimated to be 3~4 times higher. Compared to the commercial Si-Ge PDs and new QD APDs (share same epi with our laser), our MRR PDs achieved comparable performance. The Si-Ge PD/APD can also achieve record high speed while their process is not compatible to the standard foundry procedure now. Our all-Si approach shares the same process with transmitter (Tx) can reduce the technical entrance level for CMOS foundry and suitable for fast-developing optical chip-level integration in the near future. This shows the potential to make the all-Si APD a standard "black-box" component in Si photonics CMOS foundry platform component libraries.

TABLE I. COMPARISON OF PDS

Device	Performance		
	Responsivity	***Bandwidth***	***Data Rate***
All-Si double MRR APD (this work)	0.4 A/W@8.4V 0.7 A/W@8.5V	47 GHz 25 GHz	80 Gb/s NRZ 128 Gb/s PAM4
All-Si single MRR APD [9]	0.007 A/W	38.7 GHz	60 Gb/s NRZ 120 Gb/s PAM4
All-Si single MRR APD [8]	3 A/W	6 GHz	20 Gb/s NRZ
All-Si single MRR APD [6]	0.23 A/W	35 GHz	56 Gb/s NRZ 112 Gb/s PAM4
Commerical Si–Ge PD [11]	0.8 A/W	40 GHz	56 Gb/s NRZ
Record high-speed Si–Ge PD [12]	0.3 A/W	265 GHz	/
QD APD [4]	0.7 A/W	17.5 GHz	32 Gb/s NRZ

IV. Conclusion

In summary, we have reported a novel all-Si double MRR structure with a high bandwidth of 55 GHz. The MRR APD exhibits a responsivity of up to ~ 1.65 A/W and three contributing mechanisms have been clarified. A dark current of 3 nA, open NRZ eye diagram of 80 Gbit/s, PAM4 eye diagram of 128 Gbit/s, and GBP of 448 GHz were demonstrated.

The double MRR structure has been verified to extend the bandwidth limitation of the conventional MRR APD. The suppressed channel crosstalk and broadband spectrum make it suitable as high-speed dense WDM all-Si receiver. This work provides a new receiver solution and proves the feasibility of using all-Si APDs to replace Si–Ge based APDs to reduce the cost and complexity, for high-density and large-scale optical chip-level integration.

References

[1] S. Bernabe, et al. "Silicon photonics for terabit/s communication in data centers and exascale computers." Solid-State Electronics 179 (2021): 107928.

[2] D. Liang, et al. "Recent progress in heterogeneous III-V-on-silicon photonic integration." Light: Advanced Manufacturing 2.1 (2021): 59-83.

[3] M. Huang, et al. "Germanium on silicon avalanche photodiode." IEEE Journal of Selected Topics in Quantum Electronics 24.2 (2017): 1-11.

[4] B. Tossoun, et al. "32 Gbps heterogeneously integrated quantum dot waveguide avalanche photodiodes on silicon." Optics Letters 46.16 (2021): 3821-3824.

[5] Y. Peng, et al. "Small-signal analysis of all-Si microring resonator photodiode." Electronics 11.2 (2022): 183.

[6] M. Sakib, et al. "A 112 Gb/s all-silicon micro-ring photodetector for datacom applications." Optical Fiber Communication Conference. Optica Publishing Group, 2020.

[7] Van, V. Optical Microring Resonators: Theory, Techniques, and Applications; CRC Press: Boca Raton, FL, USA, 2016.

[8] Y. Peng, et al. "All-silicon microring avalanche photodiodes with a> 65 A/W response." Optics Letters 48.5 (2023): 1315-1318.

[9] Y. Yuan, et al. “An O-Band All-Silicon Microring Avalanche Photodiode with > 38 GHz Bandwidth.” In progress.

[10] Y. Yuan, et al. "Development and Modeling of Ge-free Microring Avalanche Photodiode in Optical Communication Band." Optical Fiber Communication Conference. Optica Publishing Group, 2022.

[11] S. Siew, et al. "Review of silicon photonics technology and platform development." Journal of Lightwave Technology 39.13 (2021): 4374-4389.

[12] S. Lischke, et al. "Ultra-fast germanium photodiode with 3-dB bandwidth of 265 GHz." Nature Photonics 15.12 (2021): 925-931.